Available online at www.sciencedirect.com
SCIENCE DIRECT®
Journal of Sound and Vibration 280 (2005) 329–357
JOURNAL OF SOUND AND VIBRATION
www.elsevier.com/locate/jsvi

Vibration analysis of simply supported beams with enhanced self-sensing active constrained layer damping treatments

J.X. Gao, W.H. Liao*

Smart Materials and Structures Laboratory, Department of Automation and Computer-Aided Engineering, The Chinese University of Hong Kong, Shatin, N.T., Hong Kong, China

Received 27 February 2003; accepted 5 December 2003

Abstract

The modal frequencies and loss factors of a simply supported beam with an enhanced active constrained layer (EACL) damping treatment are derived by the extended Hamilton principle and Rayleigh–Ritz method while open- and closed-loop control (displacement and velocity feedback) systems are considered. The effects of the edge element stiffness in EACL on the sensing ability, modal frequencies and loss factors of the system are investigated. The vibration characteristics for the systems with fully and partially covered passive constrained layer damping, active constrained layer damping, and EACL treatments, are discussed and compared. The effects of several key parameters such as control gain, location and coverage of the self-sensing actuators on the system performance are also studied. The results show that the enhanced self-sensing active constrained layer damping treatment is an effective way for vibration control while some important physical insights are discussed.

1. Introduction

The active constrained layer (ACL) damping treatments [1–6] have been explored to improve the damping ability of the classical passive constrained layer (PCL) damping treatments. A typical ACL treatment generally consists of a piece of passive viscoelastic material (VEM) sandwiched between an active piezoelectric layer and the base structure. With a proper control, the shear deformation of the VEM can be increased and thus the energy dissipation can be enhanced by the active action of the piezoelectric coversheet. However, it is also recognized that the viscoelastic layer will degrade the active control authority of the piezoelectric actuator being applied to the

*Corresponding author. Tel.: +852-2609-8341; fax: +852-2603-6002.
E-mail address: whliao@cuhk.edu.hk (W.H. Liao).

0022-460X/$ - see front matter © 2004 Elsevier Ltd. All rights reserved.
doi:10.1016/j.jsv.2003.12.019

base structure when compared to a purely active control, due to the reduction of the transmissibility between the piezoelectric actuator and the base structure [4]. To remedy for the transmissibility reduction problem due to the softness of the viscoelastic layer, other hybrid damping configurations, such as separate active and passive designs [7] or enhanced active constrained layer (EACL) concept [8], were proposed. It has been shown by Liao and Wang [9], that the EACL is an effective approach to solve the problem of actuator-structure transmissibility reduction. Recently, Liu and Wang [10,11] studied the static and dynamic longitudinal motions of the piezoelectric coversheet in the EACL, and major factors that affect the EACL damping characteristics were examined by assuming strain distribution in the base structure.

Dosch et al. [12] proposed a self-sensing piezoelectric actuator for collocated control and developed bridge circuits to extract the sensor signal from the actuator control voltage. In the self-sensing actuator configuration, the piezoelectric element is used simultaneously as both a sensor and an actuator. Since separate sensors are not needed, space requirement and weight penalty are reduced. Shen and Yellin [3,13] introduced the self-sensing technique into the ACL to form a self-sensing active constrained layer (SACL) damping treatment. They have shown that the SACL will eliminate system instability by ensuring that the power dissipated by the active damping always remains positive. However, the sensing and actuating abilities of the piezoelectric layer will be degraded due to the transmissibility reduction problem. Wong and Liao [14] has experimentally verified that the edge elements in the EACL can significantly improve the sensing and actuating abilities of the piezoelectric element, and an enhanced self-sensing active constrained layer (ESACL) damping treatment can provide an effective means for structural vibration control.

2. Problem statement and objective

In the previous studies by Liao and Wang [9], the piezoelectric constraining layer in the EACL treatment was used as an actuator only, and overall damping effects instead of loss factors on different vibration modes were investigated for the cantilever beam with EACL. In the recent work by Liu and Wang [10], strain distributions of the host structure were assumed to be known in order to obtain closed form solutions. However, it is difficult to find the accurate strain distribution of a beam under given boundary condition. Thus, it is hard to understand the physical insights to the actual configuration while analyzing the effects of location and coverage of the EACL treatment. In addition, the sensing ability and modal frequencies were not studied in their paper. Although Wong and Liao [14] implemented an ESACL damping treatment on the cantilever beam structure, the characteristics of the ESACL treatment have not yet been explored in depth. In particular, the sensing abilities as well as modal frequencies and loss factors of the beam system with the EACL under open- and closed-loop controls have not been investigated. The objective of this paper is to conduct a comprehensive investigation of the above issues for a simply supported beam with PCL, ACL and EACL treatments. The vibration characteristics for the beam systems with fully and partially covered PCL, ACL, and EACL treatments under open- and closed-loop displacement and velocity controls will be discussed and compared. The effects of several key parameters such as control gain, edge element stiffness, location and coverage of the self-sensing actuators on the system performances will also be studied.

3. System description and formulation

3.1. Basic relationships

The ESACL configuration is shown in Fig. 1. The host structure is attached by a VEM layer, which is constrained by a piezoelectric coversheet. A pair of edge elements mounted at both ends of the piezoelectric coversheet are used to connect the piezoelectric element directly to the host structure. The geometry and material of the edge element can be designed and selected to have different stiffness. The edge elements are modelled as equivalent springs (see Fig. 2). The purpose of these edge elements is to increase the transmissibility of the active action and sensing capability. The system model is derived based on the following assumptions:

1. The beam discussed in this paper is an Euler–Bernoulli beam.
2. The rotational inertia is negligible. The shear deformations in the piezoelectric layer and the base beam are also negligible.
3. Passive damping is only considered due to the shear deformation of the VEM. The VEM has a complex shear modulus: $G_s^* = G_s(1 + i\eta_s)$, where G_s and η_s are the shear modulus and loss factor of the material.
4. There is perfect continuity at the interfaces and no slip occurs between the layers.
5. The transverse displacement $w(x, t)$ is assumed to be the same for all layers.
6. Linear theories of elasticity, viscoelasticity and piezoelectricity are used.

A beam with a partially covered ESACL damping treatment shown in Fig. 2 is considered. The geometry and deformation of the sandwich beam are shown in Fig. 3. The continuity of displacements at the interface between the viscoelastic core and the face layers requires that the following relations hold:

$$u_s = u_b - \frac{h_s + h_b}{2}\frac{\partial w}{\partial x} + \frac{h_s}{2}\gamma_s,$$

$$u_c = u_b - h\frac{\partial w}{\partial x} + h_s\gamma_s, \qquad h = \tfrac{1}{2}(h_c + h_b) + h_s. \tag{1}$$

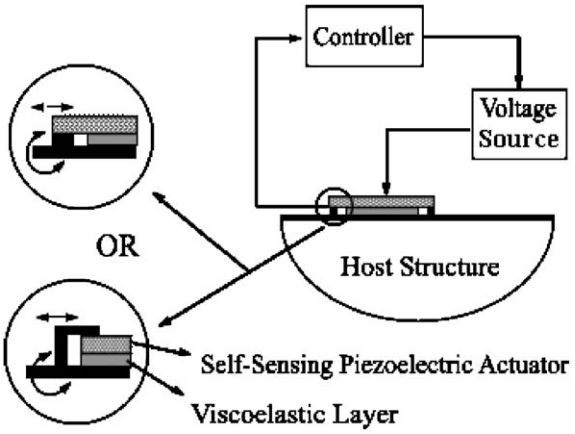

Fig. 1. Structure with enhanced self-sensing ACL.

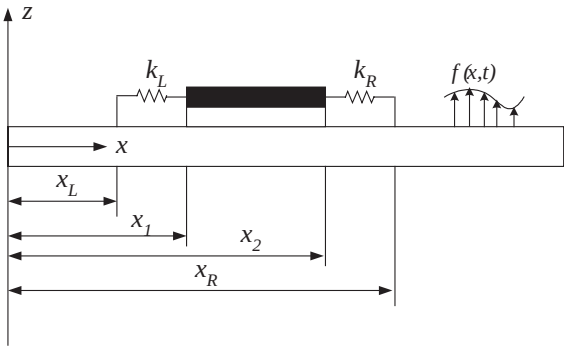

Fig. 2. Beam with partially covered EACL.

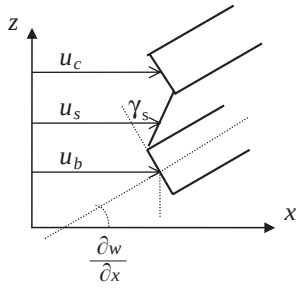

Fig. 3. Geometry and deformation of a sandwich beam.

Then,

$$\gamma_s = \frac{1}{h_s}\left[u_c - u_b + h\frac{\partial w}{\partial x}\right],$$

where u_c, u_s, and u_b are the mid-plane displacements of the piezoelectric, viscoelastic and base layers along the x-axis, respectively. γ_s is the shear strain of the VEM.

Based on the Euler–Bernoulli beam theory, the strains in piezoelectric and base layers can be expressed as follows:

$$\varepsilon_c = \frac{\partial u_c}{\partial x} - z_c\frac{\partial^2 w}{\partial x^2}, \qquad \varepsilon_b = \frac{\partial u_b}{\partial x} - z_b\frac{\partial^2 w}{\partial x^2}, \tag{2}$$

where z_b and z_c are the vertical displacements from the mid-planes of base and piezoelectric layers, respectively. The piezoelectric material considered here is transversely isotropic and its one-dimensional constitutive equations are

$$\sigma_c = Y_c\varepsilon_c - e_{31}E_3 = Y_c\left(\frac{\partial u_c}{\partial x} - z_c\frac{\partial^2 w}{\partial x^2}\right) - e_{31}E_3,$$

$$D_3 = e_{31}\varepsilon_c + \in_{33}E_3 = e_{31}\left(\frac{\partial u_c}{\partial x} - z_c\frac{\partial^2 w}{\partial x^2}\right) + \in_{33}E_3, \tag{3}$$

where Y_c is the elastic modulus, E_3 and D_3 are electric field and electric displacement along the polarization direction, e_{31} and $\in_{33}$ are the piezoelectric coefficient and dielectric constant, respectively. Since the piezoelectric layer is thin, E_3 is assumed to be independent of z,

$$E_3 = E_3(x, t). \tag{4}$$

Only transverse vibration of the beam is considered and the inertia forces in the x direction are neglected for all layers. A free body diagram of the base beam is shown in Fig. 4.

The equilibrium condition along the x direction is

$$\frac{\partial F}{\partial x}\,\mathrm{d}x - S = 0, \tag{5}$$

where F is the resultant force in the x direction, $F = \int_{A_b} \sigma_b \,\mathrm{d}A = A_b Y_b \,\partial u_b/\partial x$ and S is the shear force from the VEM, $S = \tau b \,\mathrm{d}x = G_s^* \gamma_s b \,\mathrm{d}x$, where b is the width of the beam. Substituting these into Eqs. (5) and (1) yields

$$\gamma_s = \frac{h_b Y_b}{G_s^*}\frac{\partial^2 u_b}{\partial x^2}, \tag{6}$$

$$u_c = u_b - h\frac{\partial w}{\partial x} + g^*\frac{\partial^2 u_b}{\partial x^2}, \tag{7}$$

where $g^* = h_s h_b Y_b / G_s^*$.

The deformations in the edge element springs will be:

Left edge element spring:

$$\Delta x_L = u_c(x_1) - u_b(x_L) + h\frac{\partial w(x_L)}{\partial x}$$

if $x_1 = x_L$,

$$\Delta x_L = h_s \gamma_s(x_1) = g^*\frac{\partial^2 u_b(x_1)}{\partial x^2}. \tag{8}$$

Right edge element spring:

$$\Delta x_R = u_c(x_2) - u_b(x_R) + h\frac{\partial w(x_R)}{\partial x}$$

if $x_2 = x_R$,

$$\Delta x_R = h_s \gamma_s(x_2) = g^*\frac{\partial^2 u_b(x_2)}{\partial x^2}. \tag{9}$$

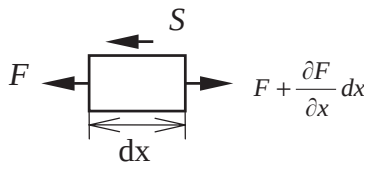

Fig. 4. Free body diagram of base beam.

3.2. The kinetic and potential energies of beam with the partially covered EACL

The potential energies of the whole system are

$$V = V_b + H_c + V_s + V_k, \tag{10}$$

where V_b is the potential energy of the base beam:

$$V_b = \int_V \sigma_b \varepsilon_b \, \mathrm{d}v = \int_0^L \frac{1}{2}\left[Y_b A_b \left(\frac{\partial u_b}{\partial x}\right)^2 + Y_b I_b \left(\frac{\partial^2 w}{\partial x^2}\right)^2 \right] \mathrm{d}x; \tag{11}$$

H_c is the electric enthalpy of the piezoelectric layer [15]:

$$\begin{aligned} H_c &= \frac{1}{2}\int [\sigma_c \varepsilon_c - E_3 D_3] \, \mathrm{d}v \\ &= \frac{1}{2}\int_{x_1}^{x_2} \left[Y_c A_c \left(\frac{\partial u_c}{\partial x}\right)^2 + Y_c I_c \left(\frac{\partial^2 w}{\partial x^2}\right)^2 \right] \mathrm{d}x - \int_{x_1}^{x_2} \left[A_c e_{31} E_3 \frac{\partial u_c}{\partial x} \right] \mathrm{d}x \\ &\quad - \frac{1}{2}\int_{x_1}^{x_2} [A_c \in_{33} E_3^2] \, \mathrm{d}x; \end{aligned} \tag{12}$$

V_s is the potential energy in the viscoelastic layer:

$$V_s = \frac{1}{2}\int_{x_1}^{x_2} A_s \tau_s (\gamma_s)^2 \, \mathrm{d}x = \frac{1}{2}\int_{x_1}^{x_2} G_s^* A_s \left(\frac{h_b Y_b}{G_s^*}\right)^2 \left(\frac{\partial^2 u_b}{\partial x^2}\right)^2 \mathrm{d}x; \tag{13}$$

V_k is the potential energy of edge elements, assuming $x_1 = x_L$, $x_2 = x_R$:

$$\begin{aligned} V_k &= \tfrac{1}{2} k_L (\Delta x_L)^2 + \tfrac{1}{2} k_R (\Delta x_R)^2 \\ &= \tfrac{1}{2} k_L (g^*)^2 \left(\frac{\partial^2 u_b(x_1)}{\partial x^2}\right)^2 + \tfrac{1}{2} k_R (g^*)^2 \left(\frac{\partial^2 u_b(x_2)}{\partial x^2}\right)^2. \end{aligned} \tag{14}$$

The kinetic energy of the transverse vibration in the overall system is

$$T = \frac{1}{2}\int_{x_1}^{x_2} (\rho_c A_c + \rho_s A_s) \left(\frac{\partial w}{\partial t}\right)^2 \mathrm{d}x + \frac{1}{2}\int_0^L \rho_b A_b \left(\frac{\partial w}{\partial t}\right)^2 \mathrm{d}x, \tag{15}$$

where ρ is the mass density, A_c, A_s, A_b, are the cross-sectional areas of the respective layers, I_c, I_b and Y_c, Y_b are the area moments of inertia and Young's moduli of the piezoelectric and base layers, respectively.

If $f(x,t)$ is the external transverse load and $Q(x,t)$ is the applied charge density per unit area to the piezoelectric layer, the virtual works done by the external load and electric charges are

$$\delta W = \int_0^L f(x,t)\delta w(x,t) \, \mathrm{d}x + \int_{x_1}^{x_2} A_c Q(x,t)\delta E_3(x,t) \, \mathrm{d}x \tag{16}$$

4. Solution for beam with partially covered EACL

Here we are interested in finding the periodic motion of the system. Assuming that harmonic loads, $f(x,t)=f_0(x)e^{i\omega t}$, $Q(x,t)=Q_c(x)e^{i\omega t}$ are applied to the system, the steady state responses will also be harmonic

$$w(x,t)=W(x)e^{i\omega t}, \qquad u_b(x,t)=U(x)e^{i\omega t}, \qquad E_3(x,t)=E(x)e^{i\omega t}. \tag{17}$$

Substituting Eq. (17) into the expressions of the potential and kinetic energies, and virtual works (Eqs. (10)–(16)), and then into the extended Hamilton principle

$$\int_{t_1}^{t_2}[\delta(T-V)+\delta W]\,dt=0. \tag{18}$$

We obtain

$$\begin{aligned}
&\delta\left\{\frac{1}{2}\int_{x_1}^{x_2}(\rho_c A_c+\rho_s A_s)W^2(x)\omega^2\,dx+\frac{1}{2}\int_0^L \rho_b A_b W^2(x)\omega^2\,dx\right\}\\
&-\delta\left\{\int_0^L\frac{1}{2}\left[Y_b A_b\left(\frac{\partial U(x)}{\partial x}\right)^2+Y_b I_b\left(\frac{\partial^2 W(x)}{\partial x^2}\right)^2\right]dx\right\}\\
&-\delta\left\{\frac{1}{2}\int_{x_1}^{x_2}\left[Y_c A_c\left(\frac{\partial U(x)}{\partial x}-h\frac{\partial^2 W(x)}{\partial x^2}+g^*\frac{\partial^3 U(x)}{\partial x^3}\right)^2+Y_c I_c\left(\frac{\partial^2 W(x)}{\partial x^2}\right)^2\right]dx\right\}\\
&+\delta\left\{\int_{x_1}^{x_2}\left[A_c e_{31}E(x)\left(\frac{\partial U(x)}{\partial x}-h\frac{\partial^2 W(x)}{\partial x^2}+g^*\frac{\partial^3 U(x)}{\partial x^3}\right)\right]dx+\tfrac{1}{2}A_c\int_{x_1}^{x_2}[\in_{33}E(x)^2]\,dx\right\}\\
&-\delta\left\{\tfrac{1}{2}k_L(g^*)^2\left(\frac{\partial^2 U(x_L)}{\partial x^2}\right)^2+\tfrac{1}{2}k_R(g^*)^2\left(\frac{\partial^2 U(x_R)}{\partial x^2}\right)^2\right\}\\
&-\delta\left\{\int_{x_1}^{x_2}G_s^* A_s\left(\frac{h_b Y_b}{G_s^*}\right)^2\left(\frac{\partial^2 U(x)}{\partial x^2}\right)^2 dx\right\}\\
&+\int_0^L f_0(x)\delta W(x)\,dx+\int_{x_1}^{x_2}A_c Q_c(x)\delta E(x)\,dx=0,
\end{aligned} \tag{19}$$

where $\int_{t_1}^{t_2}e^{2i\omega t}\,dt$, being non-zero, is factored out. The governing equations of motion for the beam with EACL can be obtained from the above variational equations. From $\delta E=0$, the charge equation yields

$$A_c e_{31}\left(\frac{\partial U(x)}{\partial x}-h\frac{\partial^2 W(x)}{\partial x^2}+g^*\frac{\partial^3 U(x)}{\partial x^3}\right)+A_c\in_{33}E(x)=A_c Q_c(x). \tag{20}$$

When the external applied charge is zero, the sensor equation due to deformation is

$$E(x)=-\frac{e_{31}}{\in_{33}}\left(\frac{\partial U(x)}{\partial x}+g^*\frac{\partial^3 U(x)}{\partial x^3}-h\frac{\partial^2 W(x)}{\partial x^2}\right). \tag{21}$$

From Eq. (21), the sensing electric field is related to the strain of the piezoelectric element, where the first two terms come from beam's axial motion and the third term is attributed to its transverse motion.

4.1. Open-loop solution

For open-loop system, there is no actuating voltage applied to the piezoelectric layer, i.e., $Q(x,t)=0$, and $f(x,t)=0$ for free vibration. In order to obtain system natural frequencies and loss factors, the displacements are approximated by modal expansion. Since the base beam is the main structure of the system, it is reasonable to choose the bending modal functions of the base beam as the expansion of the transverse displacements, and the longitudinal modal functions of a bar for the axial displacements:

$$W(x)=\sum_{n=1}^{N} w_n W_n(x), \qquad U(x)=\sum_{n=1}^{N} u_n U_n(x). \tag{22}$$

When simply supported boundary condition is considered for the open-loop case, the displacements to satisfy the boundary condition may be taken in the forms

$$W(x)=\sum_{n=1}^{N} w_n \sin(\beta_n x), \qquad U(x)=\sum_{n=1}^{N} u_n \cos(\beta_n x), \qquad \beta_n=\frac{n\pi}{L}. \tag{23}$$

4.1.1. Natural frequencies and loss factors of the system

Although there is no actuating voltage applied to the piezoelectric layer, there is sensing electric field on the piezoelectric layer and the form is shown in Eq. (21). The Rayleigh–Ritz method is employed. Substituting Eqs. (21) and (22) into Eq. (19), taking variation of energy functions with respect to the undetermined coefficients, $w_1, w_2, \ldots, w_n$; $u_1, u_2, \ldots, u_n$, and then equating these coefficients to zero, will result in an eigenvalue equation

$$\left\{ \begin{bmatrix} M & 0 \\ 0 & 0 \end{bmatrix} \omega^2 - \begin{bmatrix} K^1 & K^2 \\ K^3 & K^4 \end{bmatrix} \right\} \begin{Bmatrix} w_n \\ u_n \end{Bmatrix} = 0, \tag{24}$$

where

$$M_{mn}=(\rho_c A_c+\rho_s A_s)\int_{x_1}^{x_2} W_m(x)W_n(x)\,\mathrm{d}x+\int_0^L \rho_b A_b W_m(x)W_n(x)\,\mathrm{d}x,$$

$$K^1_{mn}=\left(Y_c I_c+Y_c A_c h^2+\frac{A_c e_{31}^2 h^2}{\in_{33}}\right)\int_{x_1}^{x_2} W_m''(x)W_n''(x)\,\mathrm{d}x+Y_b I_b\int_0^L W_m''(x)W_n''(x)\,\mathrm{d}x,$$

$$K^2_{mn}=-\left(Y_c A_c h+\frac{A_c e_{31}^2 h}{\in_{33}}\right)\int_{x_1}^{x_2} W_m''(x)[U_n'(x)+g^* U_n'''(x)]\,\mathrm{d}x,$$

$$K^3_{mn}=-\left(Y_c A_c h+\frac{A_c e_{31}^2 h}{\in_{33}}\right)\int_{x_1}^{x_2} W_n''(x)[U_m'(x)+g^* U_m'''(x)]\,\mathrm{d}x,$$

$$K^4_{mn} = \left(Y_c A_c + \frac{A_c e_{31}^2}{\in_{33}} \right) \int_{x_1}^{x_2} [U'_m(x) + g^* U'''_m(x)][U'_n(x) + g^* U'''_n(x)]\,\mathrm{d}x + \frac{A_s h_b^2 Y_b^2}{G_s^*} \int_{x_1}^{x_2} U''_m(x) U''_n(x)\,\mathrm{d}x + Y_b A_b \int_0^L U'_m(x) U'_n(x)\,\mathrm{d}x + k_L (g^*)^2 [U''_m(x_1) U''_n(x_1)] + k_R (g^*)^2 [U''_m(x_2) U''_n(x_2)]. \quad (25)$$

The relations between the undetermined coefficients w_n and u_n can be obtained from Eq. (24)

$$\{u_n\} = -[K^4]^{-1}[K^3]\{w_n\}. \quad (26)$$

Eliminating the terms u_n from Eq. (24), results in a standard eigenvalue problem, from which the eigenfrequencies and the vectors of eigenfunctions can be obtained:

$$\{[K] - \omega^2[M]\}\{w_n\} = 0, \quad (27)$$

where

$$[K] = [K^1] - [K^2][K^4]^{-1}[K^3].$$

The eigenfrequencies will be complex since there is a complex shear modulus in the viscoelastic material. After the complex eigenfrequencies have been found, the modal frequencies and loss factors of the system can be calculated as follows [16]:

$$\omega = \sqrt{\mathrm{Re}(\omega^*)^2}, \qquad \eta = \frac{\mathrm{Im}[(\omega^*)^2]}{\mathrm{Re}[(\omega^*)^2]}. \quad (28)$$

4.1.2. Sensing ability of the piezoelectric element

Substituting Eq. (22) into Eq. (21), the sensing electric field becomes

$$E(x) = -\frac{e_{31}}{\in_{33}} \left(\frac{\partial U(x)}{\partial x} - h \frac{\partial^2 W(x)}{\partial x^2} + g^* \frac{\partial^3 U(x)}{\partial x^3} \right) = -\frac{e_{31}}{\in_{33}} \sum_{n=1}^{N} [(U'_n(x) + g^* U'''_n(x))u_n - h W''_n(x) w_n]. \quad (29)$$

Substituting Eq. (23) into Eq. (29) and using Eq. (26), the sensing equation for the simply supported beam becomes

$$E(x) = -\frac{e_{31}}{\in_{33}} \sum_{n=1}^{N} [(g^* \beta_n^3 - \beta_n)u_n + h\beta_n^2 w_n] \sin(\beta_n x) = -\frac{e_{31}}{\in_{33}} \sum_{n=1}^{N} E_{sn} \sin(\beta_n x), \quad (30)$$

where the sensing electric field eigenvectors can be obtained from E_{sn}, and an index $\bar{E}_{sn}$ is introduced to express modal sensing ability

$$E_{sn} = (g^* \beta_n^3 - \beta_n)u_n + h\beta_n^2 w_n,$$

$$\bar{E}_{sn} = \sqrt{\mathrm{Re}^2(E_{sn}) + \mathrm{Im}^2(E_{sn})}. \tag{31}$$

4.2. Closed-loop solution

When an impulse is applied to the structure with a self-sensing piezoelectric actuator, the charge developed by structural deformation on the piezoelectric layer can be found by integrating the electric displacement D_3 in Eq. (3) over the electrode area:

$$\begin{aligned} q(t) &= \int_A D_3 \, \mathrm{d}A = \int_{x_1}^{x_2} e_{31} h_c \left(\frac{\partial u_c}{\partial x} - z_c \frac{\partial^2 w}{\partial x^2} \right) \mathrm{d}x \\ &= \int_{x_1}^{x_2} e_{31} h_c \left(\frac{\partial U(x)}{\partial x} + g^* \frac{\partial^3 U(x)}{\partial x^3} - h \frac{\partial^2 W(x)}{\partial x^2} \right) \mathrm{e}^{\mathrm{i}\omega t} \, \mathrm{d}x. \end{aligned} \tag{32}$$

The output sensing voltage can be obtained by dividing the charge by the sensor capacitance C_p [12],

$$V_s = \frac{q}{C_p} = \int_{x_1}^{x_2} \frac{e_{31} h_c}{\in_{33} L_c} \left(\frac{\partial U(x)}{\partial x} + g^* \frac{\partial^3 U(x)}{\partial x^3} - h \frac{\partial^2 W(x)}{\partial x^2} \right) \mathrm{e}^{\mathrm{i}\omega t} \, \mathrm{d}x, \tag{33}$$

where the L_c is the length of the piezoelectric layer.

The signal can be amplified and fed back using an appropriate controller. The displacement and velocity feedback controllers are employed in this paper.

4.2.1. Displacement feedback control

When displacement controller is used, the feedback actuating electric field to the piezoelectric layer becomes

$$\begin{aligned} E(x,t) &= G_d V_s(x,t)/h_c \\ &= \int_{x_1}^{x_2} \frac{G_d e_{31}}{\in_{33} L_c} \left(\frac{\partial U(x)}{\partial x} + g^* \frac{\partial^3 U(x)}{\partial x^3} - h \frac{\partial^2 W(x)}{\partial x^2} \right) \mathrm{e}^{\mathrm{i}\omega t} \, \mathrm{d}x, \end{aligned} \tag{34}$$

where G_d is the gain of displacement feedback control.

Substituting Eqs. (34) and (22) into (19), the eigenvalue equation will be obtained as done in the open-loop case, since the displacement feedback control law changes the system stiffness only:

$$\left\{ \begin{bmatrix} M & 0 \\ 0 & 0 \end{bmatrix} \omega^2 - \begin{bmatrix} K_d^1 & K_d^2 \\ K_d^3 & K_d^4 \end{bmatrix} \right\} \begin{Bmatrix} w_n \\ u_n \end{Bmatrix} = 0, \tag{35}$$

$$M_{mn} = (\rho_c A_c + \rho_s A_s) \int_{x_1}^{x_2} W_m(x) W_n(x) \, \mathrm{d}x + \int_0^L \rho_b A_b W_m(x) W_n(x) \, \mathrm{d}x,$$

$$K^1_{dmn} = (Y_c I_c + Y_c A_c h^2 + G_{fd} h^2) \int_{x_1}^{x_2} W''_m(x) W''_n(x)\,\mathrm{d}x + Y_b I_b \int_0^L W''_m(x) W''_n(x)\,\mathrm{d}x,$$

$$K^2_{dmn} = -(Y_c A_c h + G_{fd} h) \int_{x_1}^{x_2} W''_m(x)[U'_n(x) + g^* U'''_n(x)]\,\mathrm{d}x,$$

$$K^3_{dmn} = -(Y_c A_c h + G_{fd} h) \int_{x_1}^{x_2} W''_n(x)[U'_m(x) + g^* U'''_m(x)]\,\mathrm{d}x,$$

$$\begin{aligned} K^4_{dmn} = {} & (Y_c A_c + G_{fd}) \int_{x_1}^{x_2} [U'_m(x) + g^* U'''_m(x)][U'_n(x) + g^* U'''_n(x)]\,\mathrm{d}x \\ & + \frac{A_s h_b^2 Y_b^2}{G_s^*} \int_{x_1}^{x_2} U''_m(x) U''_n(x)\,\mathrm{d}x + Y_b A_b \int_0^L U'_m(x) U'_n(x)\,\mathrm{d}x \\ & + k_L (g^*)^2 [U''_m(x_1) U''_n(x_1)] + k_R (g^*)^2 [U''_m(x_2) U''_n(x_2)], \end{aligned}$$

$$G_{fd} = \frac{h_c e_{31}^2}{\in_{33}} G_d \left(\frac{G_d}{2} + 1 \right). \tag{36}$$

4.2.2. Velocity feedback control

When velocity controller is used, the feedback actuating electric field to the piezoelectric layer yields

$$\begin{aligned} E(x,t) = {} & -G_v \frac{\partial V_s(x,t)/h_c}{\partial t} \\ = {} & \int_{x_1}^{x_2} \frac{G_d e_{31}(\mathrm{i}\omega)}{\in_{33} L_c} \left(\frac{\partial U(x)}{\partial x} + g^* \frac{\partial^3 U(x)}{\partial x^3} - h \frac{\partial^2 W(x)}{\partial x^2} \right) \mathrm{e}^{\mathrm{i}\omega t}\,\mathrm{d}x, \end{aligned} \tag{37}$$

where G_v is the gain of velocity feedback control.

Substituting Eqs. (37) and (22) into (19), we can obtain

$$\left\{ \begin{bmatrix} M & 0 \\ 0 & 0 \end{bmatrix} \omega^2 - \begin{bmatrix} C^1 & C^2 \\ C^3 & C^4 \end{bmatrix} \omega - \begin{bmatrix} K_v^1 & K_v^2 \\ K_v^3 & K_v^4 \end{bmatrix} \right\} \begin{Bmatrix} w_n \\ u_n \end{Bmatrix} = 0. \tag{38}$$

The condition for a non-trivial solution of Eq. (38) requires

$$\left| \begin{bmatrix} M & 0 \\ 0 & 0 \end{bmatrix} \omega^2 - \begin{bmatrix} C^1 & C^2 \\ C^3 & C^4 \end{bmatrix} \omega - \begin{bmatrix} K_v^1 & K_v^2 \\ K_v^3 & K_v^4 \end{bmatrix} \right| = 0, \tag{39}$$

where

$$M_{mn} = (\rho_c A_c + \rho_s A_s) \int_{x_1}^{x_2} W_m(x) W_n(x)\,\mathrm{d}x + \int_0^L \rho_b A_b W_m(x) W_n(x)\,\mathrm{d}x,$$

$$C^1_{mn} = \mathrm{i} G_{fv} h^2 \int_{x_1}^{x_2} W''_m(x) W''_n(x)\,\mathrm{d}x,$$

$$C_{mn}^2 = -\mathrm{i}G_{fv}h\int_{x_1}^{x_2} W_m''(x)[U_n'(x) + g^* U_n'''(x)]\,\mathrm{d}x,$$

$$C_{mn}^3 = C_{mn}^2,$$

$$C_{mn}^4 = \mathrm{i}G_{fv}h\int_{x_1}^{x_2} [U_m'(x) + g^* U_m'''(x)][U_n'(x) + g^* U_n'''(x)]\,\mathrm{d}x,$$

$$K_{vmn}^1 = (Y_c I_c + Y_c A_c h^2)\int_{x_1}^{x_2} W_m''(x)W_n''(x)\,\mathrm{d}x + Y_b I_b\int_0^L W_m''(x)W_n''(x)\,\mathrm{d}x,$$

$$K_{vmn}^2 = -Y_c A_c h\int_{x_1}^{x_2} W_m''(x)[U_n'(x) + g^* U_n'''(x)]\,\mathrm{d}x,$$

$$K_{vmn}^3 = K_{vmn}^2,$$

$$\begin{aligned} K_{vmn}^4 = {} & Y_c A_c\int_{x_1}^{x_2} [U_m'(x) + g^* U_m'''(x)][U_n'(x) + g^* U_n'''(x)]\,\mathrm{d}x \\ & + \frac{A_s h_b^2 Y_b^2}{G_s^*}\int_{x_1}^{x_2} U_m''(x)U_n''(x)\,\mathrm{d}x + Y_b A_b\int_0^L U_m'(x)U_n'(x)\,\mathrm{d}x \\ & + k_L(g^*)^2[U_m''(x_1)U_n''(x_1)] + k_R(g^*)^2[U_m''(x_2)U_n''(x_2)], \end{aligned}$$

$$G_{fv} = \frac{h_c e_{31}^2}{\in_{33}} G_v. \tag{40}$$

Having obtained the complex eigenfrequencies of the system from Eq. (39), the natural frequencies and loss factors of the system can be calculated by using Eq. (28).

5. Results and discussions

5.1. Comparisons with results in the literature

To validate the analytical formulation presented in this paper, one example from Lall et al. [17] will be analyzed first. The materials of base beam and cover layer are the same, $Y_b = Y_c = 207$ GPa, $\rho_b = \rho_c = 7.8 \times 10^3$ kg/m^3, viscoelastic material has complex shear modulus $G_s^* = 2.615 \times 10^5(1 + 0.38\mathrm{i})$ Pa, $\rho_s = 2.0 \times 10^3$ kg/m^3, the dimension of the beam $L = 0.3$ m, $h_c = 0.5$ mm, $h_s = 2.5$ mm, $h_b = 5.0$ mm.

Lall et al. studied a simply supported beam partially covered with a passive damping patch, which is similar to the configuration shown in Fig. 2 but no edge elements exist. The formulations in this paper can be used to analyze this example. For the present study, analytical solutions are obtained by using the first 10 flexural and longitudinal displacement modal functions. Table 1 gives natural frequencies and loss factors of the fully covered beam system and Table 2 shows the first modal frequencies and loss factors of partially covered beam with different coverage ratios: $(x_2 - x_1)/L = 20\%$, 40% and 60% at different positions. It can be seen from Tables 1 and 2 that

Table 1
Comparison between Lall et al. and present approach for fully covered sandwich beam

Mode	Results from Lall et al. [17]		Results in this paper	
	Frequency (rad/s)	Loss factor	Frequency (rad/s)	Loss factor
1	740.6	4.48×10^{-3}	740.6	4.50×10^{-3}
2	2948.3	1.15×10^{-3}	2949.0	1.10×10^{-3}
3	6629.7	5.12×10^{-4}	6629.7	5.13×10^{-4}
4	11782.6	2.89×10^{-4}	11783.0	2.89×10^{-4}

Table 2
The first modal frequency and loss factor of partially covered sandwich beam from Lall et al. and present approach

Position	Percent coverage	Results from Lall et al. [17]		Results in this paper	
		Frequency (rad/s)	Loss factor	Frequency (rad/s)	Loss factor
1	20.0	811	0.614×10^{-5}	811	0.638×10^{-5}
	40.0	789	0.167×10^{-3}	788	0.174×10^{-3}
	60.0	759	0.929×10^{-3}	759	0.950×10^{-3}
2	20.0	793	0.398×10^{-4}	792	0.412×10^{-4}
	40.0	768	0.363×10^{-3}	767	0.372×10^{-3}
	60.0	748	0.124×10^{-2}	748	0.130×10^{-2}
3	20.0	782	0.600×10^{-4}	782	0.611×10^{-4}
	40.0	768	0.363×10^{-3}	758	0.456×10^{-3}
	60.0	744	0.136×10^{-2}	744	0.140×10^{-2}

the results obtained from the present method are very close to the those given by Lall et al., except for that with 40% coverage at position 3 in Table 2, which value may be miss typed in the paper by Lall et al.

5.2. Natural frequencies of the base beam

The configuration of the simply supported beam system with EACL is shown in Fig. 2. The geometric and material properties used in calculations are given below. The material of the base beam is aluminum, which $Y_b = 70$ GPa and $\rho_b = 2.71 \times 10^3$ kg/m^3. The piezoelectric material is PZT-5H, which $Y_c = 49$ GPa, $\rho_c = 7.5 \times 10^3$ kg/m^3, $e_{31} = -6.5$ C/m^2, and $\in_{33} = 1.3 \times 10^{-8}$ F/m. The VEM used here has complex shear modulus of $G_s^* = 0.896 \times 10^6(1 + 0.5\mathrm{i})$ Pa and $\rho_s = 1.0 \times 10^3$ kg/m^3. The dimensions of the system are $L = 0.3$ m, $b = 0.03$ m, $h_c = 0.5$ mm, $h_s = 1.0$ mm, and $h_b = 4.0$ mm. The length and location of the EACL, the stiffness of the edge elements, and the gain of the feedback control can be varied.

Since the base beam is the main structure of the system, the natural frequencies of the system are mainly dependent on the base layer. The frequencies of the simply supported beam can be

obtained from $\omega_n = (n^2\pi^2/L^2)\sqrt{Y_3 I_3/(\rho_3 A_3)}$. Based on this, one can obtain $\omega_1 = 644.0$ rad/s, $\omega_2 = 2574.0$ rad/s, $\omega_3 = 5792.0$ rad/s, and $\omega_4 = 10297.0$ rad/s, which are identical to those calculated by the approach presented in this paper.

5.3. Open-loop system characteristics

5.3.1. Natural frequencies and loss factors of the fully covered beams

The natural frequencies and loss factors of the base beam, the beam with fully covered PCL (coversheet is piezoelectric material, but no piezoelectric effect is considered, i.e., $e_{31} = 0$), the beam with EPCL (PCL with edge elements), the beam with ACL (piezoelectric effect is considered but no edge elements), and EACL (ACL with edge elements) are shown in Table 3. It can be seen that the PCL treatment makes modal frequencies decrease and induces significant loss factors into the system comparing to those of the base beam. It is also noticed that the piezoelectric effect can slightly increase the natural frequencies and loss factors comparing ACL to PCL and EACL to EPCL, even the difference is not significant. It can also be found that the effect of the edge elements on the natural frequencies and loss factors is evident, the natural frequencies increase but loss factors decrease significantly with the increase of the edge element stiffness, especially for lower modes. It is understood that the edge elements make the whole system stiffer and the VEM becomes more difficult to deform.

5.3.2. Natural frequencies and loss factors of the partially covered beams

The piezoelectric patch is set at two positions on the base beam for partial coverage: Location 1 as $x_1 = 0.0$ m and $x_2 = x_1 + 0.06$ m; Location 2 at the center of the beam, i.e., $x_1 = 0.12$ m and $x_2 = x_1 + 0.06$ m. In both cases, the length of the treatment remains 6 cm, which is 20% coverage. The natural frequencies and loss factors of the beams with partially covered PCL, EPCL, ACL

Table 3
Natural frequencies and loss factors of beams with fully covered PCL, EPCL, ACL and EACL

	Mode 1		Mode 2		Mode 3		Mode 4	
	Frequency (rad/s)	Loss factor	Frequency (rad/s)	Loss factor	Frequency (rad/s)	Loss factor	Frequency (rad/s)	Loss factor
Base beam only	644.0	0	2574.0	0	5792.0	0	10297.0	0
Beam with PCL	586.4	0.0612	2206.4	0.0242	4893.4	0.0119	8653.2	0.0069
Beam with EPCL								
$k_L = k_R = 10^6$ N/m	599.0	0.0477	2230.6	0.0222	4918.0	0.0115	8681.2	0.0067
$k_L = k_R = 10^7$ N/m	644.1	0.0161	2365.4	0.0129	5008.0	0.0125	8850.5	0.0061
Beam with ACL	587.1	0.0633	2206.6	0.0245	4893.5	0.0119	8653.2	0.0069
Beam with EACL								
$k_L = k_R = 10^7$ N/m	648.4	0.0170	2370.0	0.0133	5011.9	0.0125	8854.9	0.0061

and EACL at locations 1 and 2 are shown in Tables 4 and 5, respectively. It is clearly shown that the partially covered PCL treatment can decrease the system frequencies and increase loss factors as discussed for the fully covered beam. The edge elements increase the system frequencies and decrease the loss factors at location 1; however, the edge elements increase the second and fourth modal loss factors at location 2. It can also be seen from Tables 4 and 5 that the loss factors of the beam with partially covered PCL or ACL are greatly related to the location of the treatment. For example, the first modal loss factor is much larger at location 2 than that at location 1; however, the second modal loss factor is larger at location 1 than that at location 2. That means we can place the patch at an appropriate location for a specific modal vibration to be controlled.

Fig. 5 shows the effects of locations (the central point position of the patch, $x = (x_1 + x_2)/2$) of the treatments (length of the treatment is 6 cm, i.e., 20% coverage) on the first four modal frequencies and loss factors of the beam with partially covered ACL and EACL. As expected, it is shown that the modal frequencies and loss factors of the beam systems vary a lot with the change of locations of these partially covered treatments on the beam. It can be seen that the modal loss factors will reach the maxima while the corresponding modal frequencies are reaching or close to the minima. It can be explained that system frequencies will be increased when the system becomes stiffer, then the loss factors will be decreased due to less VEM deformation. It can also be found that the edge element stiffness has great effect on the frequencies and loss factors. The edge elements can increase frequencies of all modes; however, they could cause loss factors decrease at some locations but increase at others. For example, shown in Fig. 5(d), the second modal loss factor of the system with EACL at the positions near to the center of the beam will be larger than that of the system with ACL. This is also shown in Table 5, which the second and fourth modal loss factors at the center will increase with the increase of the edge element stiffness. Similar phenomena can be observed for the third and higher modal loss factors at other locations. It is interesting to note that the edge elements with stiffness $k_L = k_R = 10^7$ N/m make the variation of the fourth modal frequency and loss factor opposite to those with the ACL as shown in Figs. 5(g) and (h).

Next, different coverage ratios of the treatments will be investigated. Fig. 6 shows the effect of different coverage ratios, $(x_2 - x_1)/L = 20\%$, 40% and 60%, respectively at different positions on the first four modal frequencies and loss factors of the beam with partially covered ACL and EACL ($k_L = k_R = 10^6$ N/m). It can be found that larger coverage ratios can cause larger loss factors and reduce the modal frequencies. It should be noted that coverage ratios can also change the patterns of the frequencies and loss factors. For example, the peak points of the third and fourth frequencies with 40% coverage reverse comparing to those with 20% coverage; similar reverse changes can be found for the second and third modal frequencies, as well as the fourth loss factor with 60% coverage comparing to those with 20% coverage. Together with the coverage and location, the edge element stiffness also has significant effect on the frequencies and loss factors. It changes not only the values of frequencies and loss factors, but also their patterns. For example, the pattern of the third modal loss factor of the EACL system with 60% coverage inverses as shown in Fig. 6(f) due to the edge elements compared to the ACL with the same coverage.

The correlation between the modal loss factors and the modal functions (mode shapes) of the base beam can be observed from Fig. 5. With 20% coverage of ACL, the modal loss factors and mode shapes are closely related because the base beam is the main structure of the system. The

Table 4
Natural frequencies and loss factors of the beams with partially covered PCL, EPCL, ACL and EACL at Location 1: $x_1 = 0$, $x_2 = x_1 + 0.06$ m

	Mode 1		Mode 2		Mode 3		Mode 4	
	Frequency (rad/s)	Loss factor	Frequency (rad/s)	Loss factor	Frequency (rad/s)	Loss factor	Frequency (rad/s)	Loss factor
Base beam only	644.0	0	2574.0	0	5792.0	0	10297.0	0
Beam with PCL	636.9	1.69×10^{-4}	2493.2	6.20×10^{-4}	5538.6	9.96×10^{-4}	9878.1	1.0×10^{-3}
Beam with EPCL $k_L = k_R = 10^7$ N/m	639.1	1.09×10^{-4}	2524.0	3.73×10^{-4}	5647.1	5.63×10^{-4}	10070.0	5.61×10^{-4}
Beam with ACL	636.9	1.70×10^{-4}	2493.2	6.21×10^{-4}	5538.6	9.98×10^{-4}	9878.2	1.0×10^{-3}
Beam with EACL $k_L = k_R = 10^7$ N/m	639.1	1.12×10^{-4}	2524.5	3.80×10^{-4}	5648.9	5.75×10^{-4}	10074.0	5.76×10^{-4}

Table 5
Natural frequencies and loss factors of the beams with partially covered PCL, EPCL, ACL and EACL at Location 2: $x_1 = 0.12$ m, $x_2 = x_1 + 0.06$ m

	Mode 1		Mode 2		Mode 3		Mode 4	
	Frequency (rad/s)	Loss factor	Frequency (rad/s)	Loss factor	Frequency (rad/s)	Loss factor	Frequency (rad/s)	Loss factor
Base beam only	644.0	0	2574.0	0	5792.0	0	10297.0	0
Beam with PCL	596.1	1.60×10^{-3}	2547.3	5.72×10^{-5}	5496.2	1.30×10^{-3}	9968.4	1.83×10^{-4}
Beam with EPCL $k_L = k_R = 10^7$ N/m	616.6	7.03×10^{-4}	2547.8	2.09×10^{-4}	5648.1	6.60×10^{-4}	9974.4	7.08×10^{-4}
The beam with ACL	596.1	1.60×10^{-3}	2547.3	5.77×10^{-5}	5496.2	1.30×10^{-3}	9968.4	1.84×10^{-4}
Beam with EACL $k_L = k_R = 10^7$ N/m	617.0	7.26×10^{-4}	2547.8	2.10×10^{-4}	5650.9	6.82×10^{-4}	9974.4	7.10×10^{-4}

modal loss factors will reach maxima at locations corresponding to the peak amplitudes of the mode shapes and minima at the nodes of the mode shapes of the base beam. For example, the first modal loss factor will be maximum when the ACL patch is placed at the center of the beam. At the same location, the second modal loss factor becomes minimum since it is the nodal point of the second mode. Comparing EACL to ACL cases, it should be noted that the edge elements can lessen the effect of the vibration nodes on the loss factors. On the other hand, it can be seen from Fig. 6 that increasing the coverage of ACL or EACL will reduce the correlation between the modal loss factors and the mode shapes of the base beam. The reason is that the stiffness and damping of the patch with larger per cent coverage (for example, 60%) ACL or EACL will have greater influence on the performance of the whole system. In these cases, the variation of the modal loss factors with respect to the location of the patch will be more complicated, especially for higher modes.

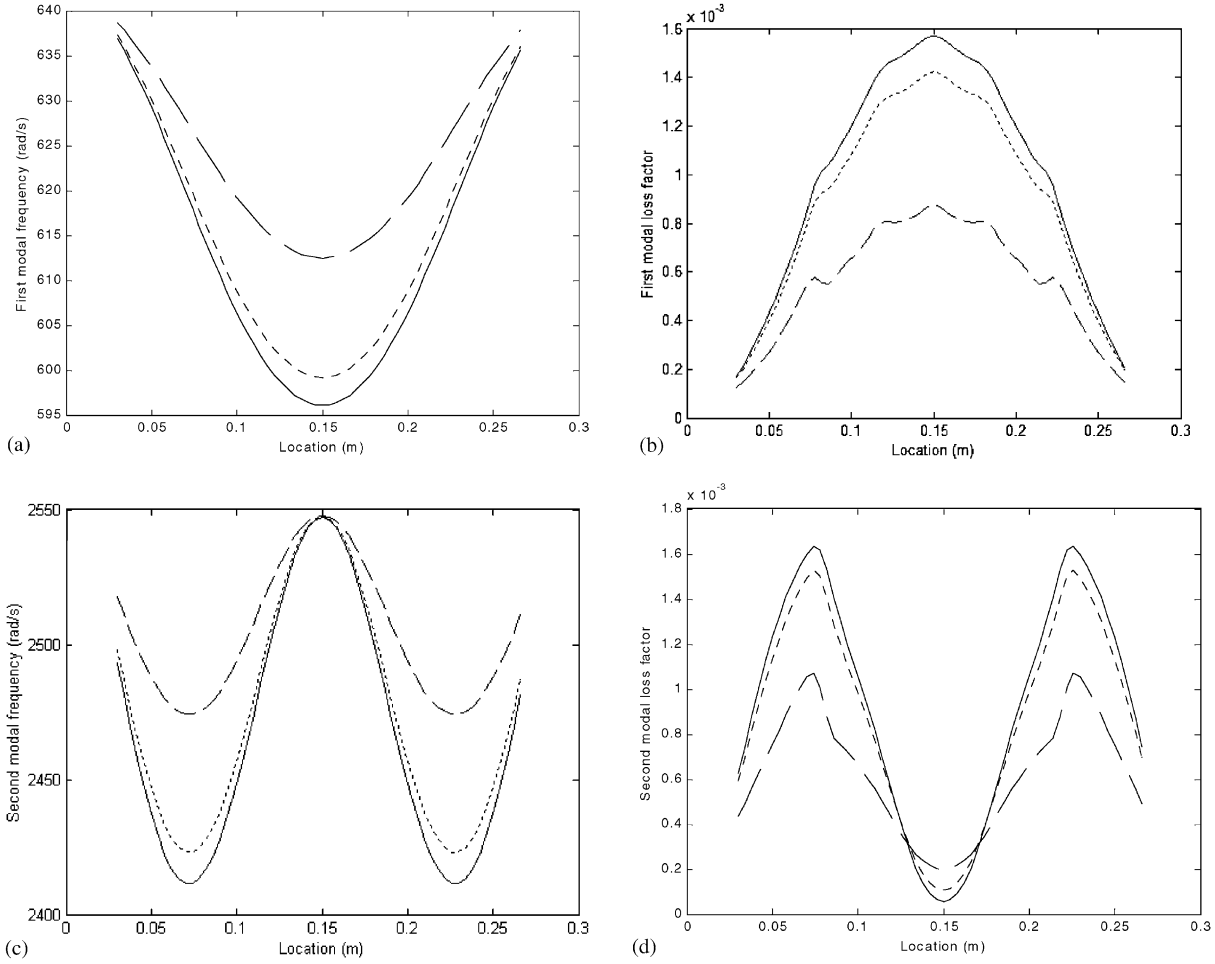

Fig. 5. Effect of location of ACL and EACL treatments (20% coverage) on the first four modal frequencies and loss factors (—— ACL, - - - - EACL with $k_L = k_R = 10^6$ N/m, – – – – EACL with $k_L = k_R = 10^7$ N/m).

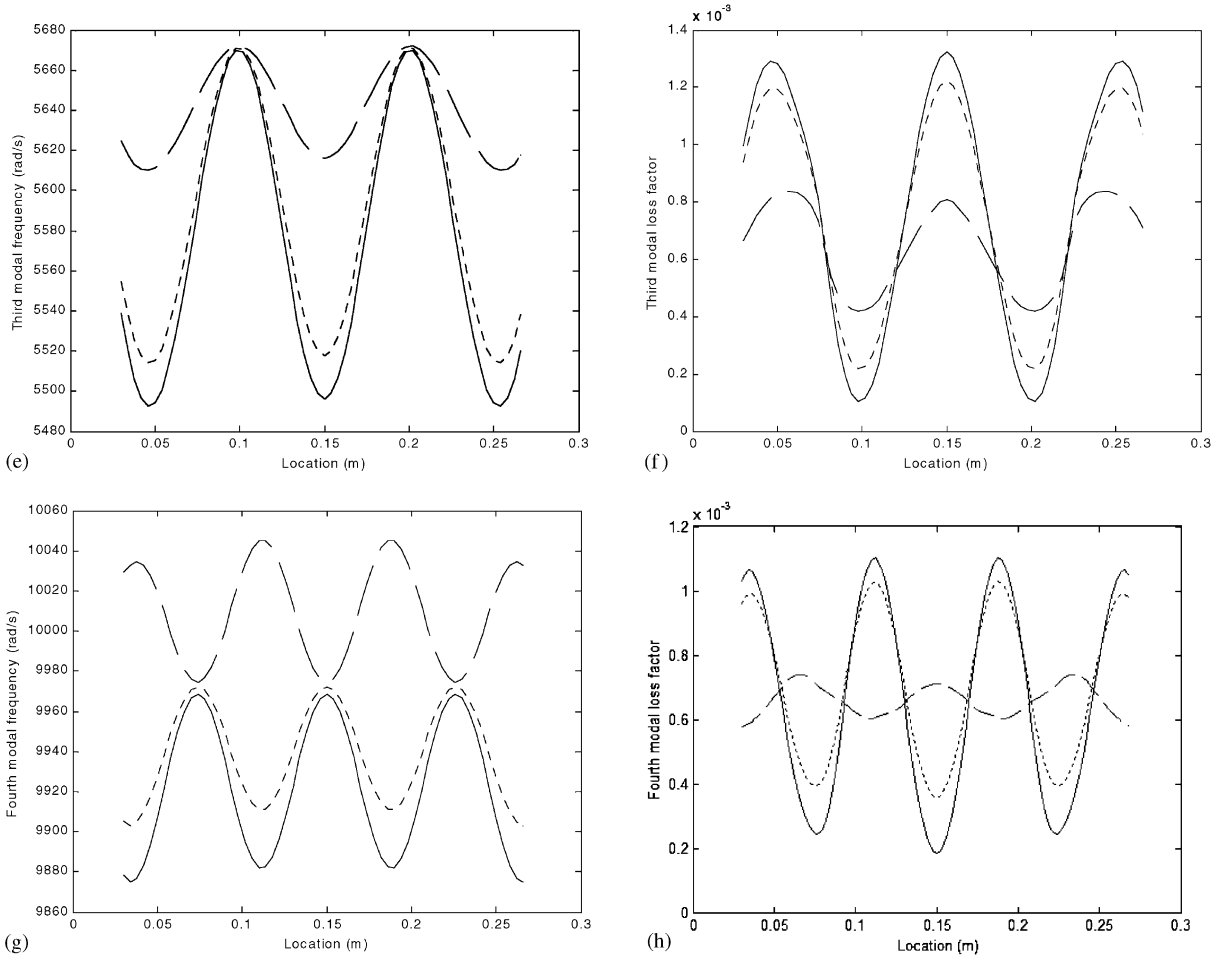

Fig. 5 (*continued*).

5.3.3. *Sensing ability of systems*

After the eigenvectors of transverse displacements have been found from Eq. (27), the eigenvectors of electric field and modal sensing ability indices can be obtained from Eq. (31). Fig. 7 shows the effect of the edge element stiffness on the first two modal sensing ability indices of the beams with fully covered EACL beam. It can be seen that the edge elements can improve the sensing ability significantly. For example, the first and second modal sensing ability indices of the EACL beam with edge element stiffness $k_L = k_R = 10^7$ N/m increase about 2.4 and 4.0 times compared to the ACL cases ($k_L = k_R = 0$). It is also clearly shown in Fig. 7 that the sensing ability of the piezoelectric element increases with the increase of the edge element stiffness. Fig. 8 shows the first two modal sensing ability indices of the piezoelectric element in the beam with 20% partially covered ACL and EACL at different location ($x = (x_1 + x_2)/2$, the central point of the patch). It is illustrated that the first and second modal sensing ability indices with edge element stiffness $k_L = k_R = 10^7$ N/m increase about 10 and 2 times comparing with the ACL beam. It is

also demonstrated that the sensing ability of the systems with partially covered ACL and EACL have close relations with position of the treatment, and the vibration modes of the base beam. It can also be found that the systems with partially covered ACL and EACL treatments can produce better modal sensing ability than that of the system with fully covered EACL for a certain mode by comparing with fully covered EACL treatment as shown in Fig. 7. For example, the second modal sensing abilities of the beam with partially covered EACL at the positions around one-fourth or three-fourths of the beam may be larger than that with fully covered EACL under the same edge element stiffness. It may be explained that some electric signals for the mode could be canceled out for the beams with fully covered ACL or EACL treatments, and therefore the fully covered ACL or EACL treatments may have worse sensing abilities than those with partially covered ACL or EACL.

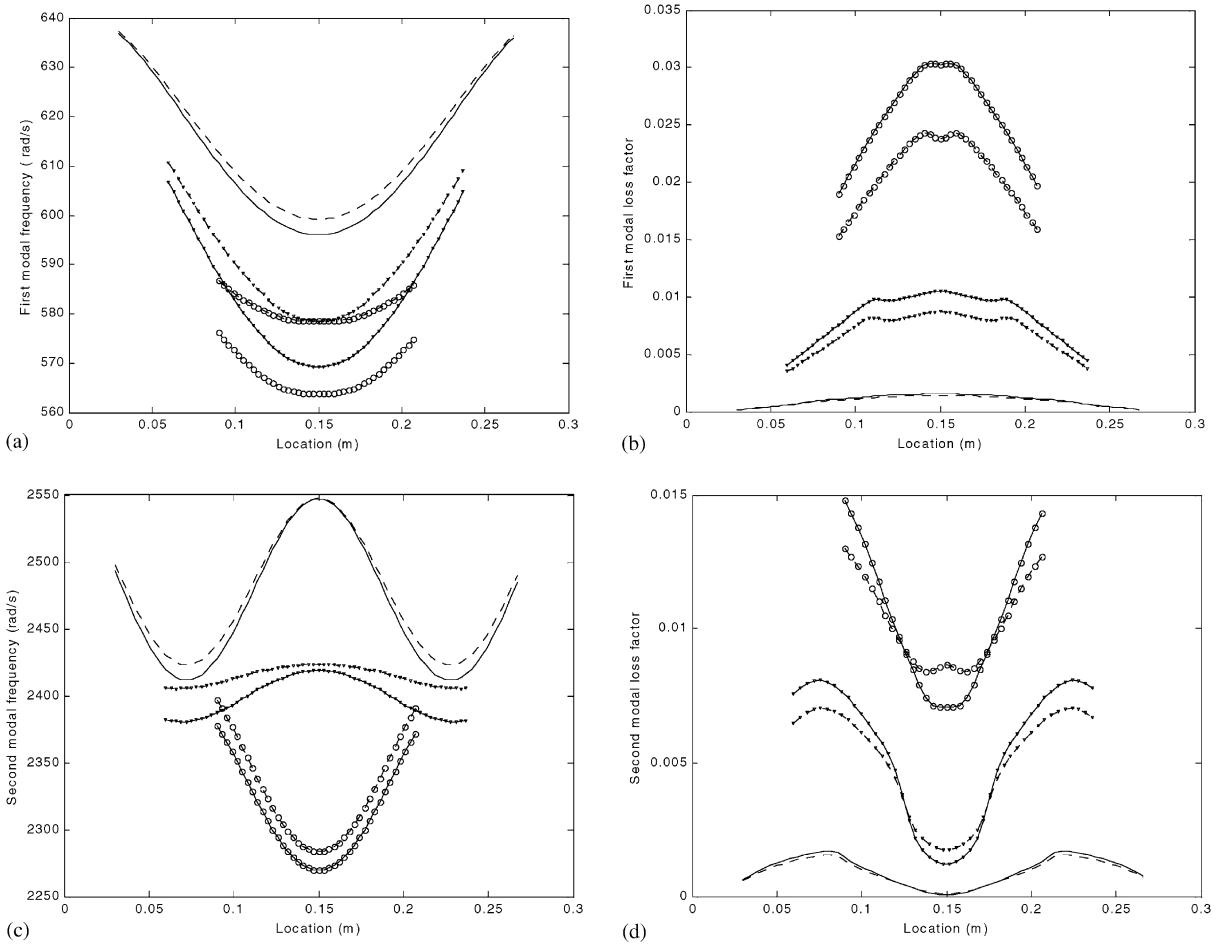

Fig. 6. The first four modal frequencies and loss factors versus different percent coverage of ACL and EACL treatments (20% coverage: —— ACL, - - - - EACL; 40% coverage: —▽— ACL, ···▽··· EACL; 60% coverage: —○— ACL, ··· ○ ··· EACL).

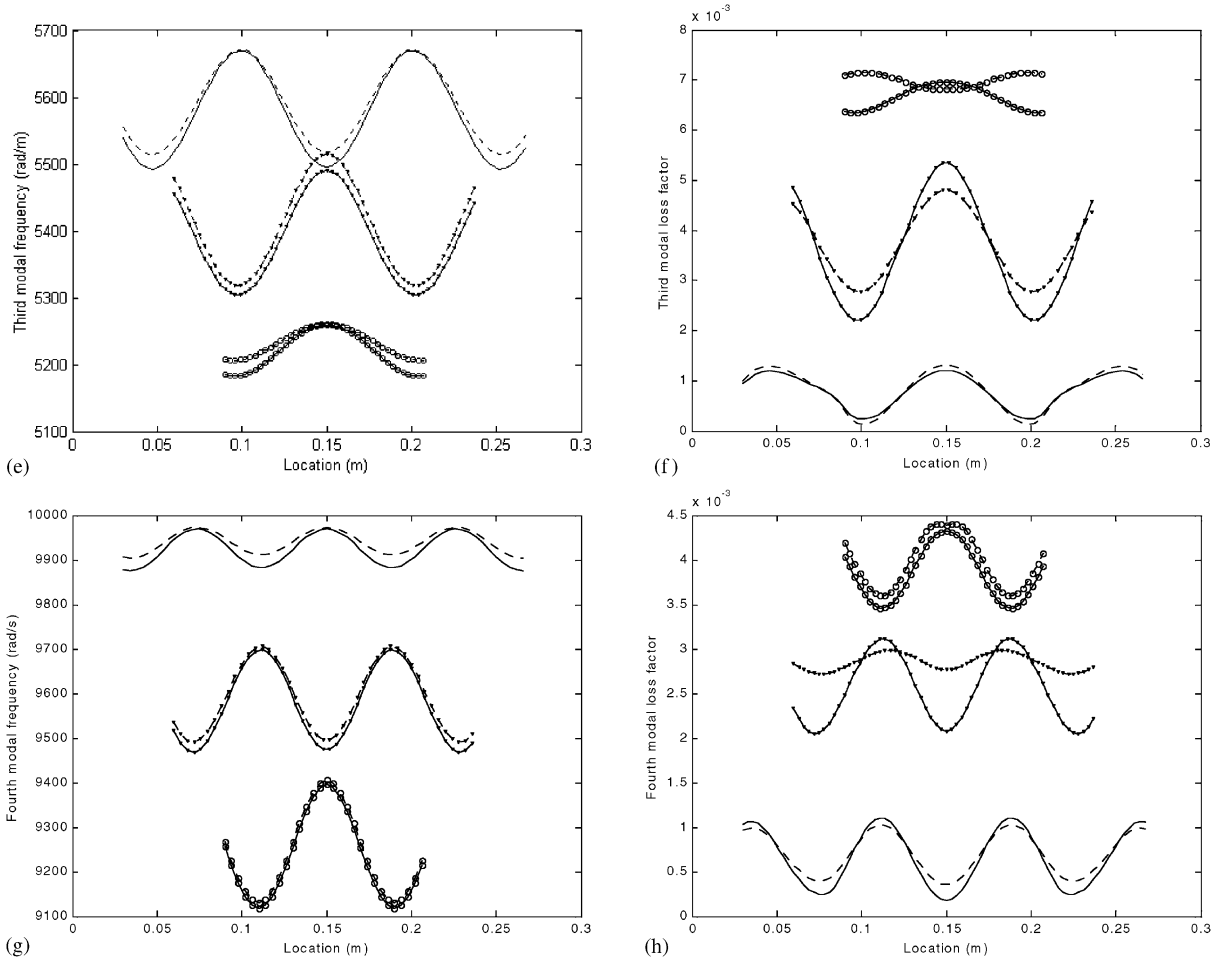

Fig. 6 (*continued*).

5.4. Closed-loop system characteristics

5.4.1. Displacement feedback control

5.4.1.1. Effect of displacement control gain and edge element stiffness. Fig. 9 shows the effect of displacement control gain and edge element stiffness on the first four modal frequencies and loss factors of the beam with partially covered ESACL at position $x_1 = 0.05$ m, $x_2 = x_1 + 0.06$ m (20% coverage). It can be found that the modal frequencies will increase significantly with the increase of the edge element stiffness, while the control gain has very little effect on the frequencies. It can also be seen that the modal loss factors increase with the increase of the displacement control gain. However, the loss factors of the first two modes decrease with the increase of edge element stiffness when the control gain is small, but increase when the control gain is getting larger. It can be explained that the passive damping dominates as the actuating voltage is small, and there is less shear deformation in the VEM layer due to the existence of the

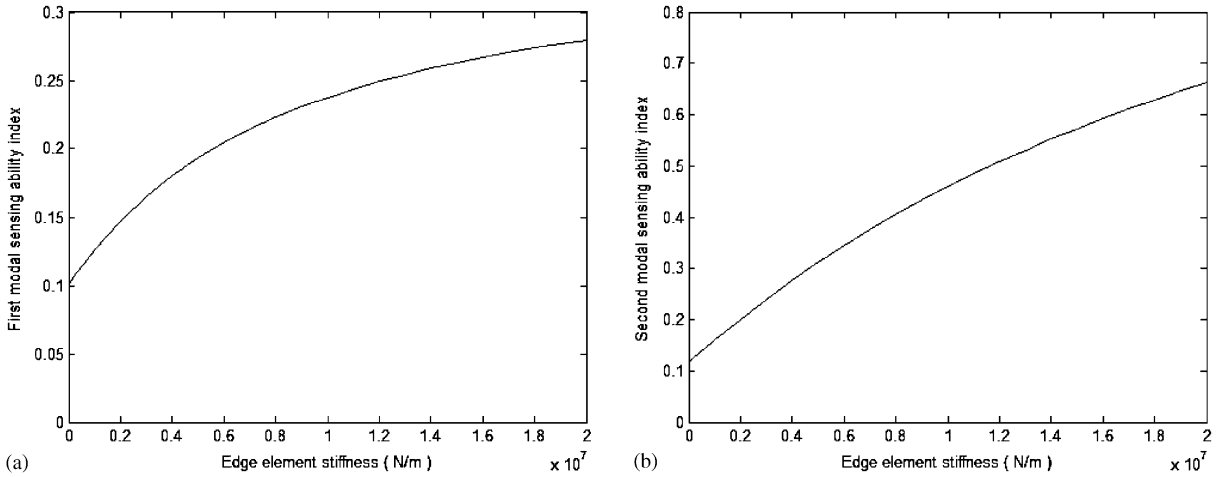

Fig. 7. The first two modal sensing ability indices of the beam with fully covered EACL versus edge element stiffness.

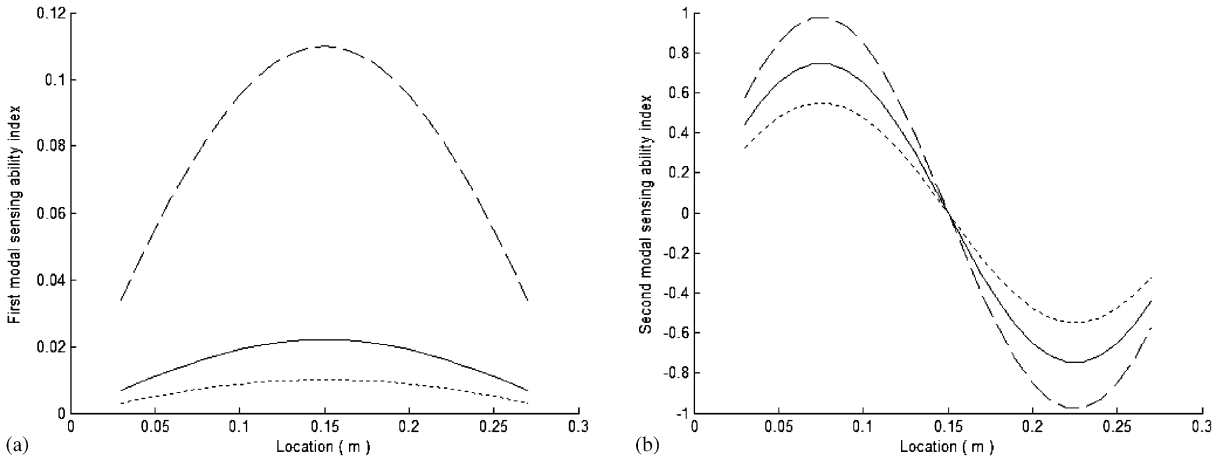

Fig. 8. The first two modal sensing ability indices of beam with partially covered ACL and EACL: - - - - ACL, —— EACL with $k_L = k_R = 10^6$ N/m, – – – – EACL with $k_L = k_R = 10^7$ N/m.

stiff edge elements, therefore the loss factors of the first two modes will be reduced with the increase of the edge element stiffness. When the control gain is getting larger, the active damping will be dominating since the active moment transmitted from the piezoelectric layer to the base beam via the edge elements becomes dominative. It indicates larger actuating/sensing abilities result in larger loss factors for active vibration control. Furthermore, for the third and fourth modes, the modal loss factors become larger with the increase of edge element stiffness no matter the control gain is small or large. In these cases, edge elements are helpful for providing both passive and active damping. This phenomenon shows that the active/passive hybrid damping characteristics of the beam with partially covered ESACL is complicated. The damping characteristics are not only dependent on the control gain and edge element stiffness, but also the

vibration modes of interest. It can also be seen from Fig. 9 that the loss factors are greatly affected by the displacement control gain, especially when the edge element stiffness is large. However, the control gains have only little effect on the loss factors for the SACL case (zero edge element stiffness). It is concluded that the loss factors of the ESACL treatment will be larger with larger control gain but higher edge element stiffness is needed.

5.4.1.2. Effect of location and coverage of SACL and ESACL treatments. The following discussions will be focused on the difference between the open- and closed-loop damping characteristics, as well as the unique phenomena for the closed-loop performance with varying location and coverage of SACL and ESACL treatments.

Fig. 10 shows the effect of different coverage ratios, $(x_2 - x_1)/L = 20\%$, 40% and 60%, respectively, at different positions on the first four modal loss factors of the beam with partially covered SACL and ESACL ($k_L = k_R = 10^6$ N/m), as the displacement control gain $G_d = 60$. It is shown that the variations of position and coverage ratios of SACL and ESACL patches have very significant effect on the modal loss factors as discussed in the open-loop control systems. It can be seen that loss factors can be greatly improved by activating the SACL and ESACL with closed-loop displacement feedback control when comparing to the systems with passive ACL and

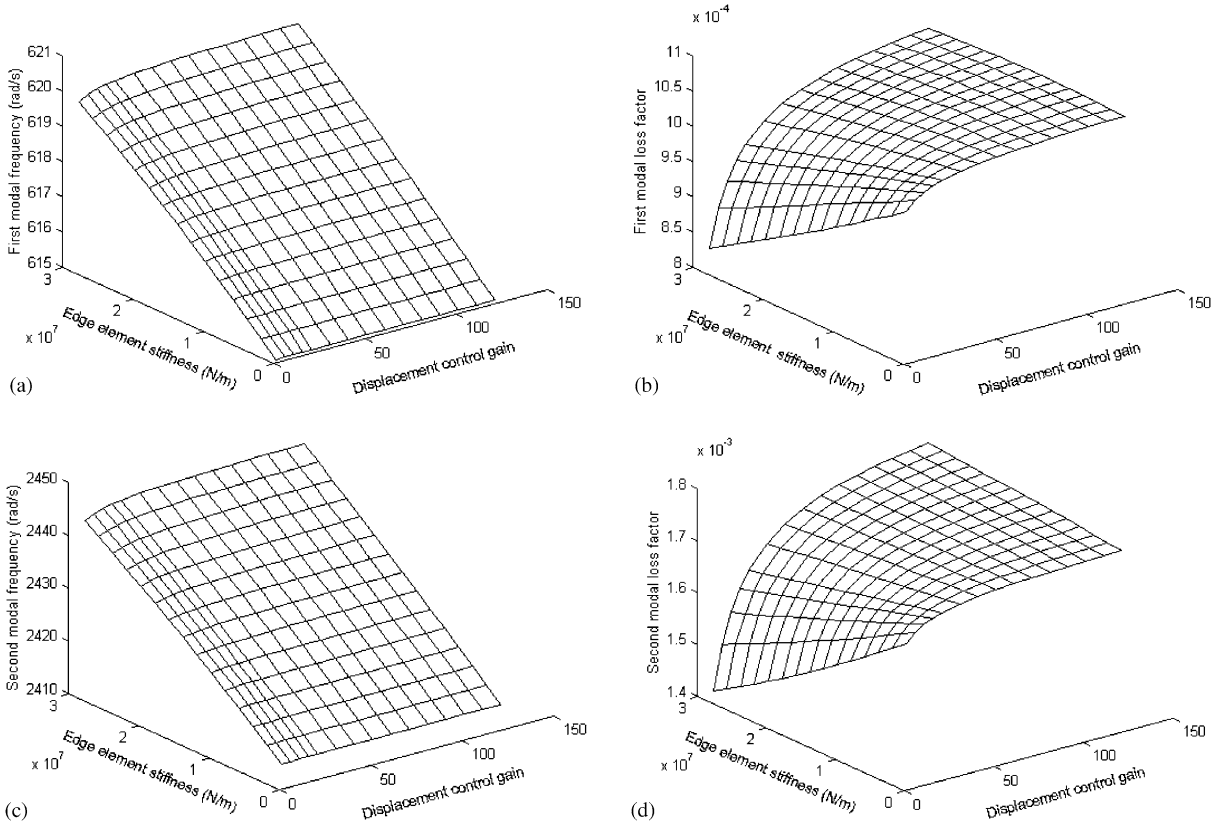

Fig. 9. Effect of displacement control gain and edge element stiffness on the first four modal frequencies and loss factors of the beam with partially covered ESACL.

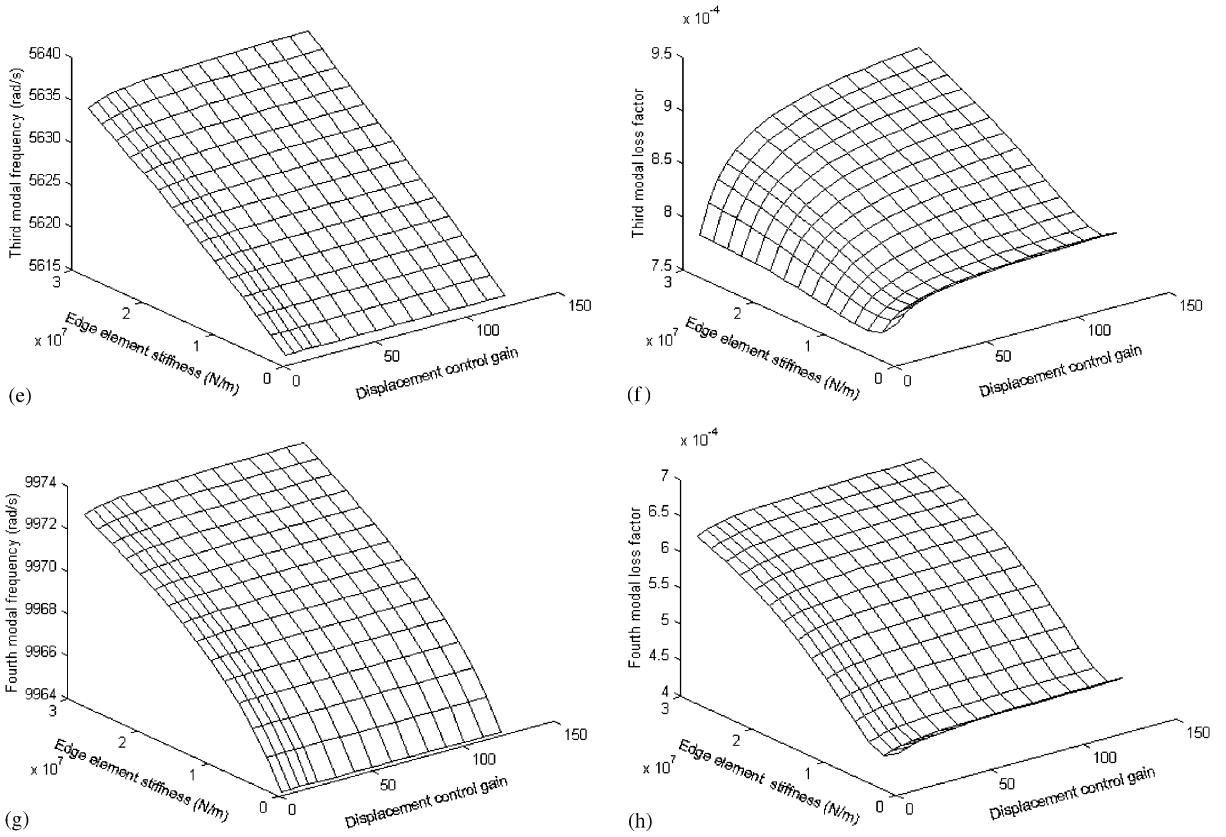

Fig. 9 (*continued*).

EACL as shown in Fig. 6. Comparing the ACL and EACL cases, the controlled loss factors of the ESACL are generally greater than those of the SACL treatment for the shown locations and coverage, even when the uncontrolled loss factors of the ACL are larger than those of the EACL as shown in Fig. 6. This shows that the edge elements in ESACL with control action can significantly improve the system loss factors as compared to the SACL treatment. The edge element stiffness also plays an important role on the values and patterns of the modal loss factors.

The loss factors shown in Fig. 10 are the hybrid loss factors that include both passive and active damping produced by SACL or ESACL treatments. It would be interesting to show the active loss factors induced by active control with SACL and ESACL treatments. The active loss factors are obtained by subtracting the open-loop passive loss factors from the hybrid loss factors. Fig. 11 shows the active loss factors of the first four modes of the systems with different coverage ratios and location of the SACL and ESACL. It can be seen that the active damping of system with SACL damping treatments can be significantly enhanced by mounting edge elements at both ends of the piezoelectric layer. The ESACL treatment can produce larger active loss factors not only for the first mode but also for higher modes. The active modal loss factors of the systems with SACL and ESACL are also greatly related to the location and coverage of the treatments. It can be found that the bigger coverage ratio can produce the larger active loss factor for the first mode,

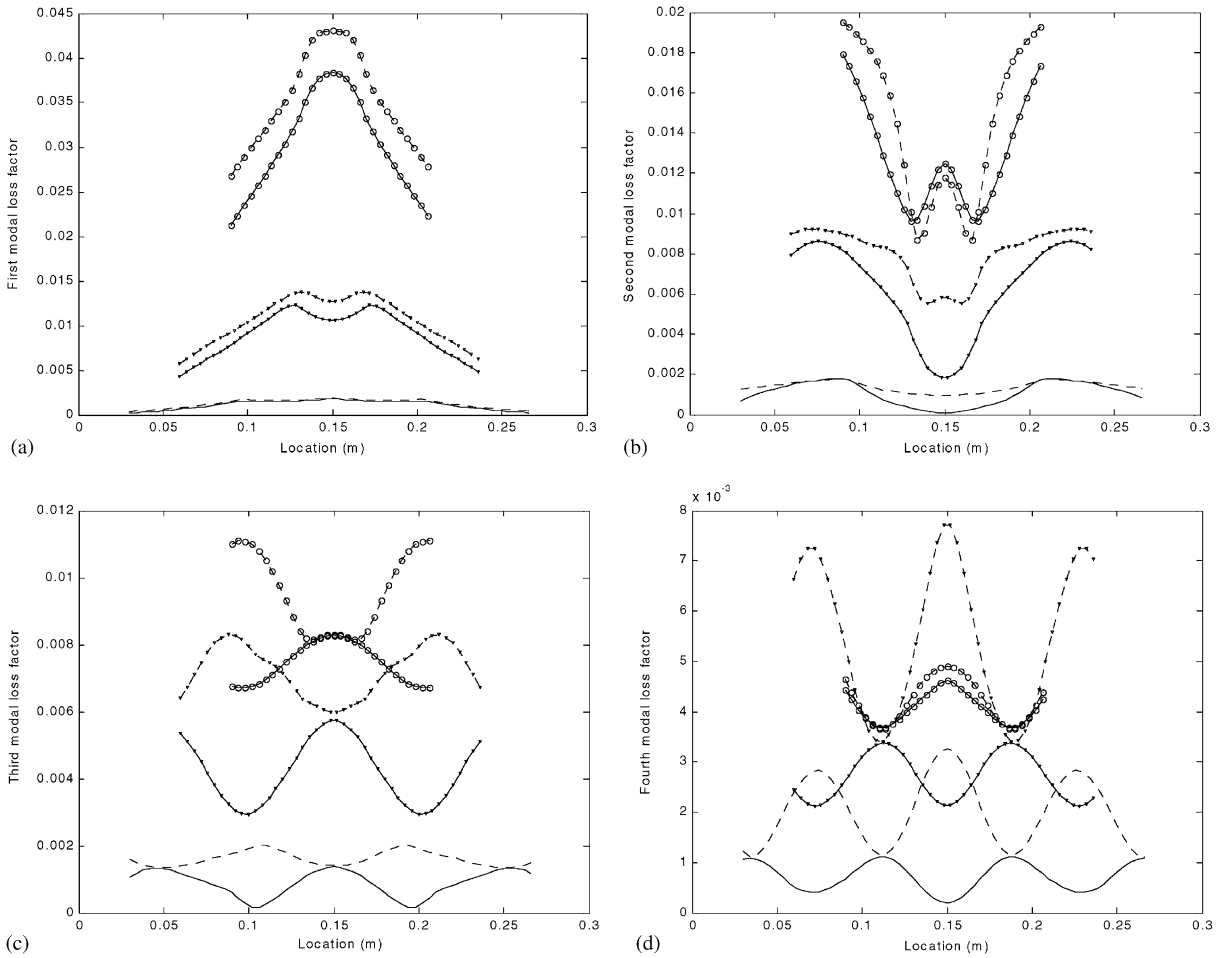

Fig. 10. Hybrid loss factors with displacement feedback versus different location and coverage of SACL and ESACL treatments (20% coverage: —— SACL, - - - - ESACL; 40% coverage: —▽— SACL, ···▽··· ESACL; 60% coverage: —○— SACL, ···○··· ESACL).

but it becomes different for the higher modes. For example, the simply supported beam with 60% coverage of ESACL can produce larger active loss factors than those of the system with 20% or 40% coverage for the first two modes; however, 40% coverage of ESACL can bring out the biggest loss factors for the third and fourth modes in the present case. It would be expected that the hybrid damping characteristics of the systems with partially covered SACL or ESACL are even more complicated, since both active and passive damping performances are not only related to the control gain and edge element stiffness, but also the location and coverage of treatments, as well as the modes of interest.

5.4.2. Velocity feedback control

5.4.2.1. Effect of control gain and edge element stiffness. Fig. 12 shows the effect of velocity control gain and edge element stiffness on the first four modal loss factors of the beam with

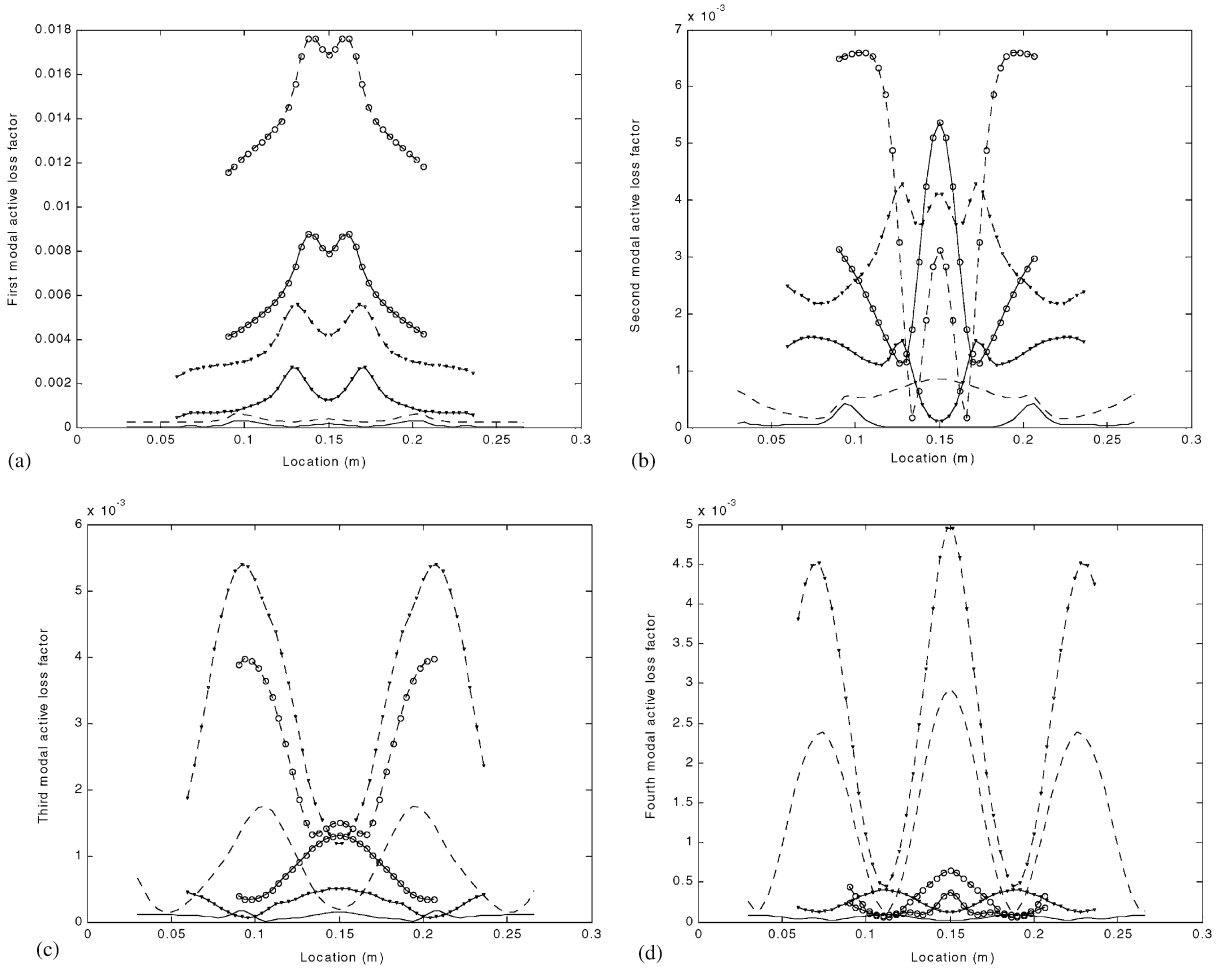

Fig. 11. Active loss factors with displacement feedback versus different location and coverage of SACL and ESACL treatments (20% coverage: —— SACL, - - - - ESACL; 40% coverage: —▽— SACL, ···▽··· ESACL; 60% coverage: —○— SACL, ···○··· ESACL).

partially covered ESACL at position $x_1 = 0.05$ m, $x_2 = x_1 + 0.06$ m (20% coverage). It can be seen from these figures that the modal loss factors will hardly vary with the increase of the control gain for the SACL system corresponding to the cases where the edge element stiffness is zero in Fig. 12. It is because the active control force from the piezoelectric layer to the base structure does not significantly increase due to the transmissibility reduction caused by the viscoelastic layer although the control voltage increases. However, with the addition of edge elements, loss factors of the ESACL system will increase with the increase of the edge element stiffness and control gain. This shows again that the ESACL treatment can effectively solve the transmissibility problem. It is also demonstrated that there exists an optimal control gain for a given edge element stiffness to maximize the loss factor of the ESACL system. It should also be noted that the loss factors could slightly decrease with the increase of the edge element stiffness as the velocity control gain is small; however, the loss factors will increase significantly with suitable control gain and edge element

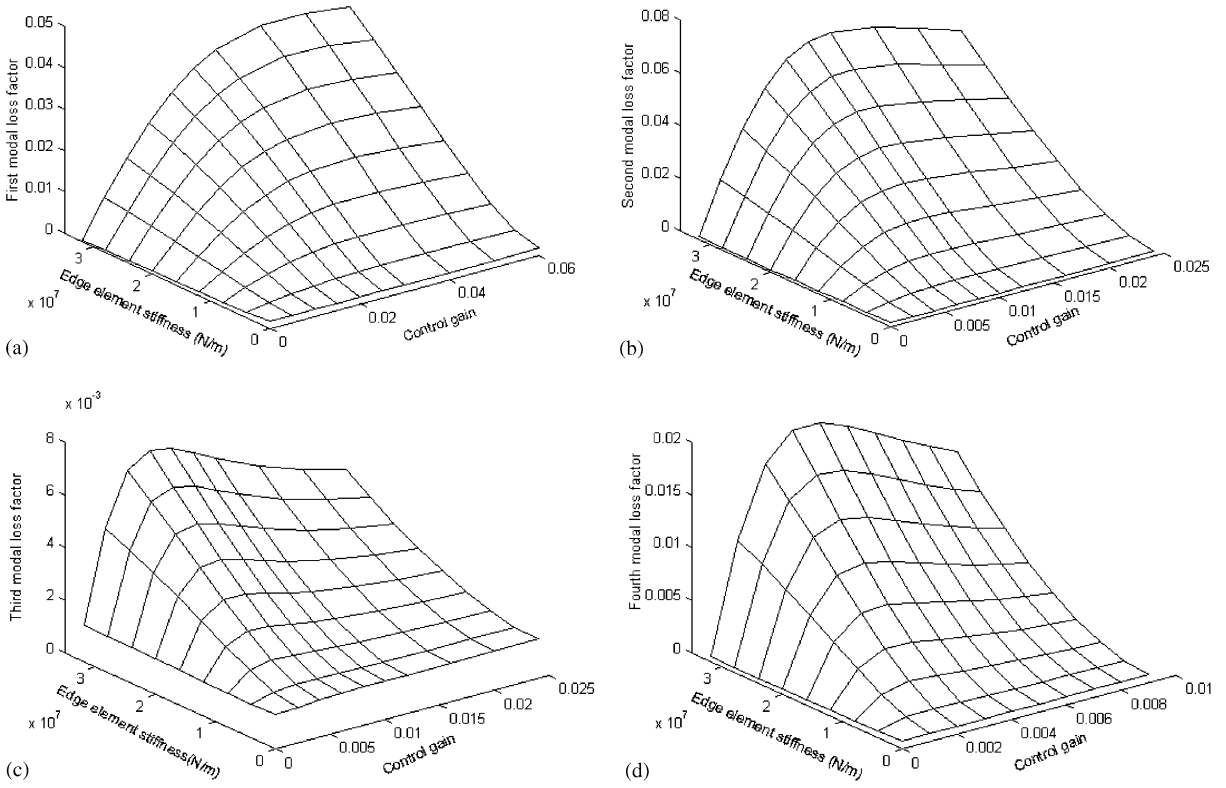

Fig. 12. Effect of velocity control gain and edge element stiffness on the first four modal loss factors of beam with partially covered ESACL.

stiffness because the stiff edge elements will bring out the control action from the actuator. It is concluded that the edge element stiffness and velocity control gain have crucial effects on the loss factors of the ESACL system and a suitable combination of the edge element stiffness and control gain can maximize the modal loss factors.

5.4.2.2. Effect of location and coverage of SACL and ESACL treatments. Fig. 13 shows the first four hybrid loss factors of system with different percent coverage 20%, 40% and 60% of the SACL and ESACL treatments at different positions of the beam with the same velocity gain $G_v = 0.01$ and edge element stiffness $k_L = k_R = 10^7$ N/m. It can be seen that the variations of position and coverage of the SACL and ESACL patches also have very significant effect on the modal loss factors as discussed in the displacement feedback control. The loss factors can be significantly improved by attaching ESACL patch with closed-loop velocity feedback control when comparing to the open-loop system. The edge elements in ESACL have significant effect on increasing the system loss factors as compared with the SACL treatment. Optimal hybrid modal loss factors for specific vibration modes of interest could be obtained by choosing location and coverage of the ESACL treatment with suitable edge elements stiffness.

In order to quantify the contribution of active action on loss factors, the first four modal active loss factors of system with different coverage of the SACL and ESACL are shown in Fig. 14,

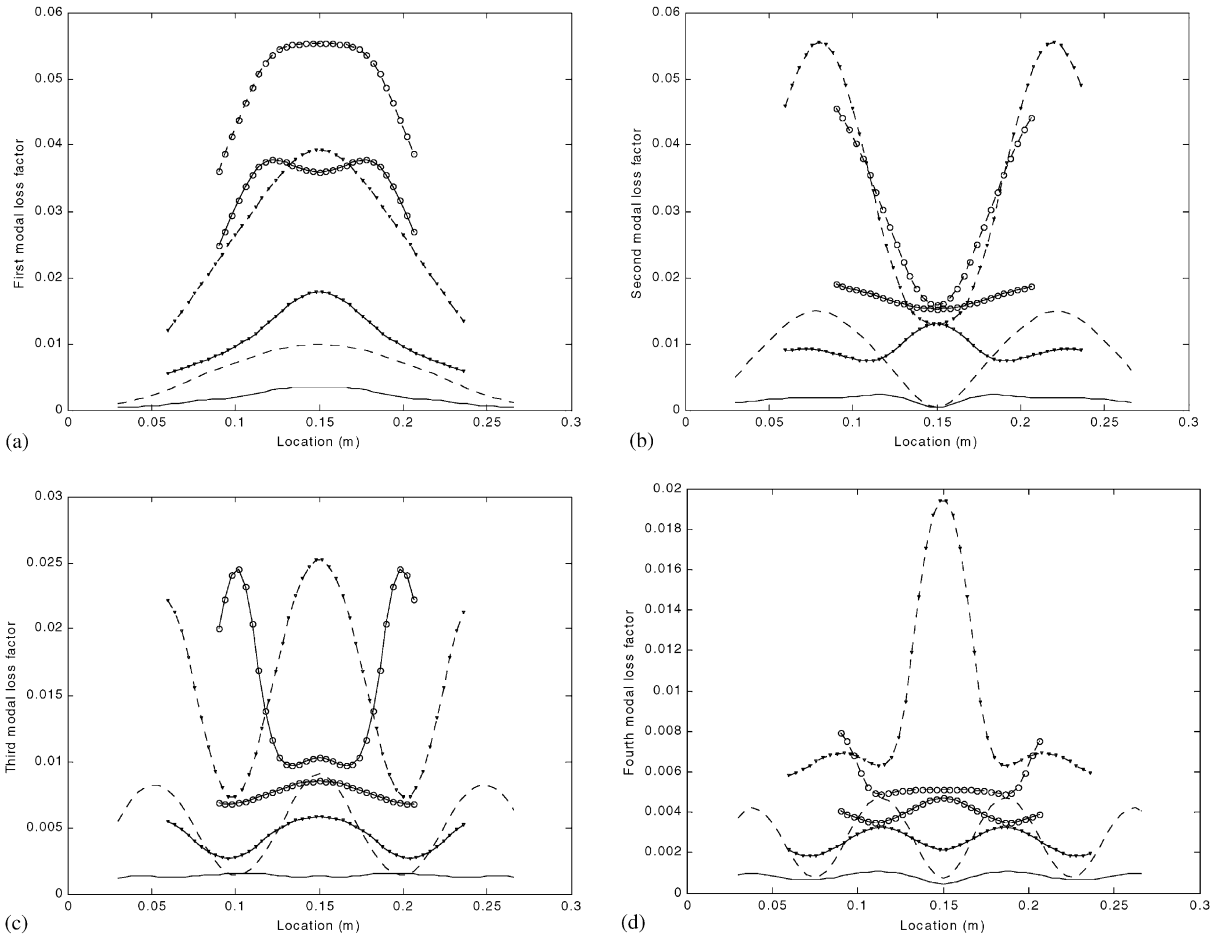

Fig. 13. Hybrid loss factors with velocity feedback versus different location and coverage of SACL and ESACL treatments (20% coverage: —— SACL, - - - ESACL; 40% coverage: —∇— SACL, ···∇··· ESACL; 60% coverage, —○— SACL, ···○··· ESACL).

which are obtained by subtracting the open-loop passive loss factors from the closed-loop hybrid loss factors. It can be seen that the ESACL treatment can produce larger active damping than the SACL system for most cases. The active loss factors of the beam with SACL and ESACL treatments are greatly related with the location and coverage of the treatments within the beam, as well as the vibration modes of interest. It can also be found that the larger coverage ratio can produce the larger loss factor for the first mode, but it may not be true for higher modes. For example, the beam with 60% ESACL coverage can have larger loss factor than that of the system with 20% or 40% coverage for the first mode; however, 40% ESACL coverage can bring out the largest loss factors for the other three modes in the present case. These phenomena are similar to the results using displacement feedback control as discussed in Section 4.3. However, their variation patterns with coverage and location are different. We can see that the velocity feedback control could generally produce larger active damping than the displacement feedback control by comparing Fig. 14 with Fig. 11, especially for the higher modes.

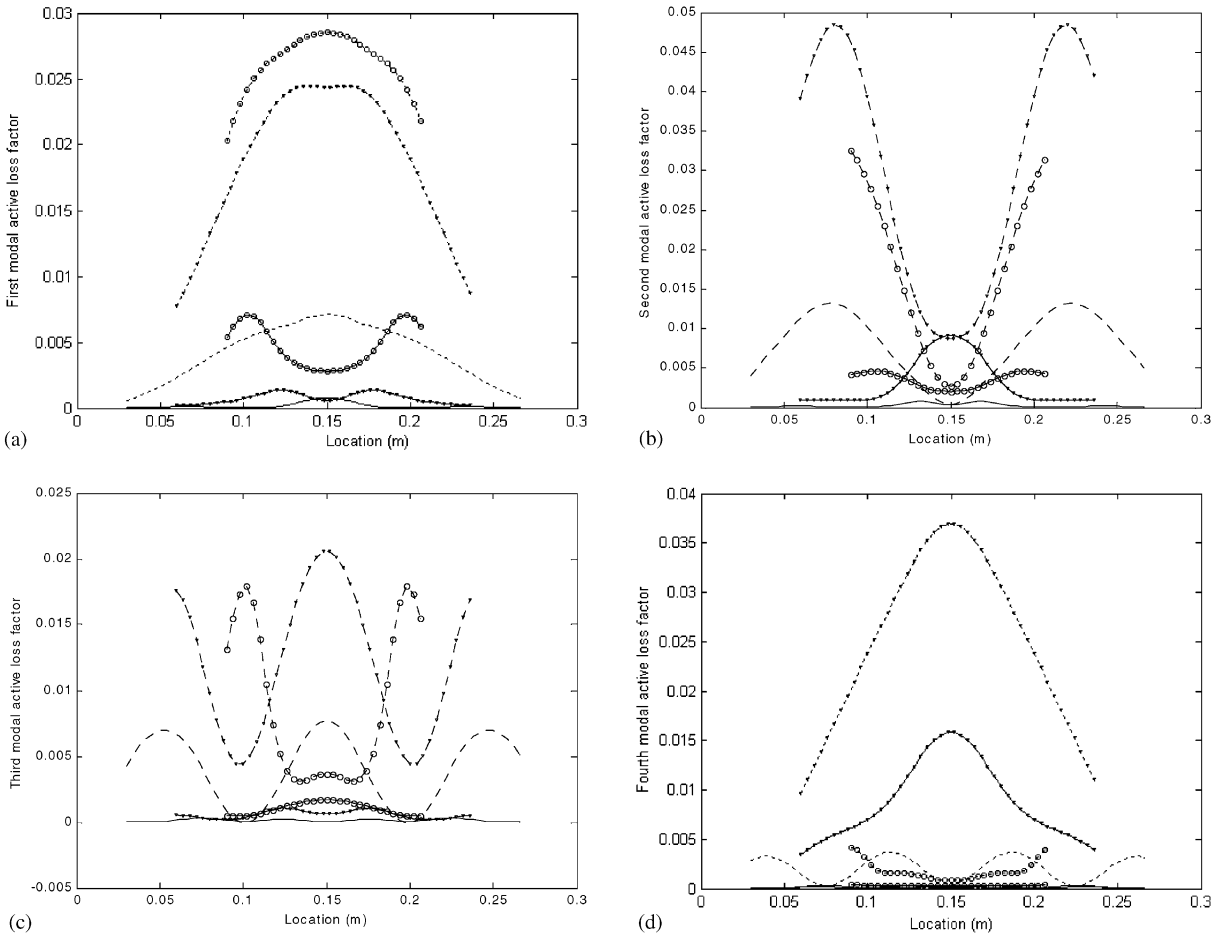

Fig. 14. Active loss factors with velocity feedback versus different location and coverage of SACL and ESACL treatments (20% coverage: —— SACL, - - - ESACL; 40% coverage: —∇— SACL, ···∇··· ESACL; 60% coverage, —○— SACL, ···○··· ESACL).

6. Conclusion

In this paper, the extended Hamilton principle and Rayleigh–Ritz method are used to analyze simply supported beams with ACL and EACL treatments. The modal frequencies and loss factors of the beam with fully or partially covered ACL and EACL are discussed while open- and closed-loop systems are considered. Simulation results show that the EACL damping treatment with self-sensing displacement or velocity feedback control is an effective means for vibration control of structures. The ESACL system can achieve much better active damping than the SACL system for most cases. The EACL treatment cannot only significantly improve the sensing ability of the piezoelectric element, but also change the modal frequencies and loss factors, which are important for practical designs of structural control systems. The location and coverage of patches have also great effect on modal frequencies and loss factors of the system with partially covered ACL or EACL for both open- and closed-loop controls. The edge element stiffness also plays a crucial role

on the system characteristics. By adjusting the feedback control gain, edge element stiffness, location and coverage of the ESACL, optimal performance for controlling vibration of a specific mode of a beam structure could be obtained.

Acknowledgements

The work described in this paper was fully supported by a grant from Research Grants Council of Hong Kong Special Administrative Region, China (Project No. CUHK4205/00E) and CUHK Postdoctoral Fellowship Scheme (00/ERG/11).

References

[1] A. Baz, J. Ro, Optimum design and control of active constrained layer damping, *American Society of Mechanical Engineers Journal of Dynamic Systems Measurement and Control, Special 50th Anniversary Design Issue* 117 (1995) 135–144.
[2] B. Azvine, G.R. Tomlinson, R.J. Wynne, Use of active constrained layer damping for controlling resonant vibration, *Smart Materials and Structures* 4 (1995) 1–6.
[3] I.Y. Shen, A variational formulation, a work-energy relation and damping mechanisms of active constrained layer treatments, *American Society of Mechanical Engineers Journal of Vibration and Acoustics* 119 (1997) 192–199.
[4] W.H. Liao, K.W. Wang, On the active–passive hybrid actions of structures with active constrained layer treatments, *American Society of Mechanical Engineers Journal of Vibration and Acoustics* 119 (1997) 563–572.
[5] S.C. Huang, D.J. Inman, E.M. Austin, Some design considerations for active and passive constrained layer damping treatments, *Smart Materials and Structures* 5 (1996) 301–313.
[6] C.H. Park, A. Baz, Vibration damping and control using active constrained layer damping: a survey, *The Shock and Vibration Digest* 31 (1999) 355–364.
[7] M.J. Lam, D.J. Inman, W.R. Saunders, Vibration control through passive constrained layer damping and active control, *Journal of Intelligent Material Systems and Structures* 8 (1997) 663–677.
[8] W.H. Liao, K.W. Wang, A new active constrained layer configuration with enhanced boundary actions, *Smart Materials and Structures* 5 (1996) 638–648.
[9] W.H. Liao, K.W. Wang, Characteristics of enhanced active constrained layer damping treatments with edge elements, Part 1: finite element model development and validation, Part 2: system analysis, *American Society of Mechanical Engineers Journal of Vibration and Acoustics* 120 (1998) 886–900.
[10] Y. Liu, K.W. Wang, A non-dimensional parametric study of enhanced active constrained layer damping treatments, *Journal of Sound and Vibration* 223 (1999) 611–644.
[11] Y. Liu, K.W Wang, Active–passive hybrid constrained layer for structural damping augmentation, *American Society of Mechanical Engineers Journal of Vibration and Acoustics* 122 (2000) 254–262.
[12] J.J. Dosch, D.J. Inman, E. Garcia, A self-sensing piezoelectric actuator for collocated control, *Journal of Intelligent Material Systems and Structures* 3 (1992) 166–185.
[13] J.M. Yellin, I.Y. Shen, A self-sensing active constrained layer damping treatment for an Euler–Bernoulli beam, *Smart Materials and Structures* 5 (1996) 628–637.
[14] K.M. Wong, W.H. Liao, Experimental investigation of an enhanced self-sensing active constrained layer damping treatment, *Proceedings of SPIE Conference on Smart Structures and Materials*, Newport Beach, CA, Vol. 4331, SPIE, Bellingham, WA, 2001, pp. 468–479.
[15] H.F. Tiersten, *Linear Piezoelectric Plate Vibrations*, Plenum Press, New York, 1969.
[16] D.K. Rao, Sandwich beams under various boundary conditions, *Journal of Mechanical Engineering Science* 20 (1978) 271–282.
[17] A.K. Lall, N.T. Asnani, B.C. Nakra, Damping analysis of partially covered sandwich beams, *Journal of Sound and Vibration* 123 (1988) 247–259.